Continuous Q1-Q1 Stokes elements stabilized with non-conforming null edge average velocity functions

Leopoldo P. Franca*, Saulo P. Oliveira†, and Marcus Sarkis‡

Abstract

We present a stabilized finite element method for Stokes equations with piecewise continuous bilinear approximations for both velocity and pressure variables. The velocity field is enriched with piecewise polynomial bubble functions with null average at element edges. These functions are statically condensed at the element level and therefore they can be viewed as a continuous Q1-Q1 stabilized finite element method. The enriched velocity-pressure pair satisfies optimal inf-sup conditions and approximation properties. Numerical experiments show that the proposed discretization outperforms the Galerkin least-squares method.

1 Introduction

The *Stokes problem*, a linear model for steady, slow-moving fluids, is a representative problem of incompressible flow. The main difficulty for approximating this problem using the Galerkin finite element method is that velocity and pressure fields are subject to the *inf-sup*, or *Babuška-Brezzi* condition [3, 6]. This compatibility constraint rules out some simple finite element pairs, such as the bilinear-velocity-pressure element [7].

In order to be able to use the bilinear-velocity-pressure pair one can stabilize the Galerkin method by adding perturbation terms which depend on the residuals of the governing equations. These strategies go back to the works [8] and [16] and have been generalized in various applications (see [13] for a review of stabilized methods for Stokes).

*Department of Mathematics, University of Colorado at Denver, PO Box 173364, Denver, CO, 80217-3364, USA.

†Departamento de Geofísica Nuclear, CPGG-UFBA, Campus Universitário da Federação, Salvador-BA, 40210-340, Brazil. Saulo Oliveira's research was sponsored by PRODOC-CAPES, Brazil.

‡Instituto Nacional de Matemática Pura e Aplicada, Estrada Dona Castorina 110, Rio de Janeiro-RJ, 22460-320, Brazil.

The bilinear-velocity-pressure pair can also be stabilized by adding conforming bubble functions to the velocity space [4, 18]. This approach requires at least three internal degrees of freedom; that is, one degree of freedom for each component of the velocity and one degree of freedom shared by both components of the velocity per element [4]. Note that the MINI element for the linear-velocity-pressure pair [2] needs only one internal degree of freedom for each component of the velocity. A wider range of bubble functions can be considered in the non-conforming case [19].

The stabilized method proposed herein introduces perturbation terms by statically condensing the non-conforming polynomial bubble functions introduced in the velocity field. These functions have null average on all edges of the quadrilateral elements and can be viewed as an extension of the conforming "quadrilateral mini" bubble functions in [4].

This work is organized as follows: Section 2 reviews the finite element formulation of the Stokes problem and introduces the proposed method. In Section 3 we prove that the method satisfies the inf-sup condition using the macroelement technique. Error estimates for both the approximate solution and its bilinear component are derived in Section 4. Section 5 reports numerical experiments and includes estimate convergence rates. Discussion and comments are presented on Section 6.

2 Finite Element Formulation

Let $\Omega \subset I\!R^2$ be an open, bounded region with smooth boundary Γ. The Stokes problem in Ω with homogeneous Dirichlet boundary conditions states that the velocity field $\boldsymbol{u}$ and the pressure field p are determined from the system of equations

$$\left\{ \begin{array}{rl} -2\mu\nabla\cdot\boldsymbol{\varepsilon}(\boldsymbol{u}) + \nabla p = \boldsymbol{f} & \text{in } \Omega, \\ \nabla\cdot\boldsymbol{u} = 0 & \text{in } \Omega, \\ \boldsymbol{u} = \boldsymbol{0} & \text{on } \Gamma, \end{array} \right. \tag{1}$$

where $\boldsymbol{\varepsilon}(\boldsymbol{u}) = (\nabla\boldsymbol{u} + (\nabla\boldsymbol{u})^t)/2$, μ is the viscosity of the fluid and $\boldsymbol{f}$ is a body force.

Let Σ be an element K, a macroelement M or the domain Ω. We denote $(v,w)_\Sigma = \int_\Sigma vw dx$, and $\|v\|_{m,\Sigma} = \|v\|_{H^m(\Sigma)}$. The subscripts are dropped unless the domain is a subset of Ω or $m > 0$. For example, $\|v\|_K = \|v\|_{0,K}$, $\|v\|_1 = \|v\|_{1,\Omega}$, and $(v,w) = (v,w)_\Omega$. Let $H_0^1(\Omega)$ be the subspace of functions of $H^1(\Omega)$ with zero trace on $\partial\Omega$ and $L_0^2(\Omega) = \{q \in L^2(\Omega)\ ;\ (q,1) = 0\}$. The variational formulation of (1) is described as: Find $\boldsymbol{u} \in V = (H_0^1(\Omega))^2$ and $p \in Q = L_0^2(\Omega)$ such that

$$\left\{ \begin{array}{lll} a(\boldsymbol{u},\boldsymbol{v}) + b(\boldsymbol{v},p) & = F(\boldsymbol{v}) & \forall\, \boldsymbol{v} \in V \\ -b(\boldsymbol{u},q) & = 0 & \forall\, q \in Q, \end{array} \right. \tag{2}$$

$$a(\boldsymbol{u},\boldsymbol{v}) = 2\mu\left(\boldsymbol{\varepsilon}(\boldsymbol{u}),\boldsymbol{\varepsilon}(\boldsymbol{v})\right), \quad F(\boldsymbol{v}) = (\boldsymbol{f},\boldsymbol{v}), \quad b(\boldsymbol{v},q) = -\left(\nabla\cdot\boldsymbol{v},q\right).$$

Let $\mathcal{T}_h(\Omega)$ be a partition of Ω into non-overlapping quadrilateral elements K. We associate with each element $K \in \mathcal{T}_h(\Omega)$ a bilinear, isoparametric transformation F_K that maps $(\hat{x},\hat{y}) \in \hat{K} = [-1,1]^2$ onto $(x,y) \in K$ as

$$\begin{cases} x = a_K^1 + b_K^1\hat{x} + c_K^1\hat{y} + d_K^1\hat{x}\hat{y} \\ y = a_K^2 + b_K^2\hat{x} + c_K^2\hat{y} + d_K^2\hat{x}\hat{y}. \end{cases} \tag{3}$$

We employ the standard quasi-uniformity and regularity assumptions [5] for $\mathcal{T}_h(\Omega)$. Thus, the Jacobian matrix

$$B_K = \begin{bmatrix} b_K^1 + d_K^1\hat{y} & c_K^1 + d_K^1\hat{x} \\ b_K^2 + d_K^2\hat{y} & c_K^2 + d_K^2\hat{x} \end{bmatrix} \tag{4}$$

satisfies $J_K := \det(B_K) \neq 0$ for $1 \leq \hat{x},\hat{y} \leq 1$. In particular, $\bar{J}_K := \det(\bar{B}_K) \neq 0$, where

$$\bar{B}_K = \begin{bmatrix} b_K^1 & c_K^1 \\ b_K^2 & c_K^2 \end{bmatrix}. \tag{5}$$

Let $Q_h \subset Q$ be defined as

$$Q_h = \{p \in Q \cap C^0(\Omega)\ ;\ p|_K = \hat{p}\circ F_K^{-1} \ \text{ on } \ K \ \text{ and } \ \hat{p} \in Q_1(\hat{K})\},$$

where $C^0(\Omega)$ is the space of continuous functions in Ω and $Q_1(\hat{K})$ is the space of bilinear functions in $\hat{K}$. For the discrete velocity field space we consider $V_h = V_h^1 \oplus V_h^E$, where

$$V_h^1 = \{\boldsymbol{v} \in V\ ;\ \boldsymbol{v}|_K := \boldsymbol{v}_K = \hat{\boldsymbol{v}}\circ F_K^{-1} \ \text{ on } \ K \ \text{ and } \ \hat{\boldsymbol{v}} \in Q_1(\hat{K})\},$$

$$V_h^E = \prod_{K\in\mathcal{T}_h(\Omega)} V_{h,K}^E, \qquad V_{h,K}^E = \Big\{\boldsymbol{v}_K \in H^1(K)\ ;\ \boldsymbol{v}_K = \bar{B}_K\hat{\boldsymbol{z}}\circ F_K^{-1}$$
$$\text{and } \ \hat{\boldsymbol{z}} = \begin{pmatrix} \alpha_K^1 \\ \alpha_K^2 \end{pmatrix}\hat{\phi} + \alpha_K^3\begin{pmatrix} \hat{y} \\ \hat{x} \end{pmatrix}\hat{\phi}\Big\}, \tag{6}$$

and $\hat{\phi}(\hat{x},\hat{y}) = (\hat{x}^2 + \hat{y}^2 - 4/3)/2$. The product of $\bar{B}_K$ by $\hat{\boldsymbol{z}}\circ F_K^{-1}$ is motivated from the proof of Theorem 3.1 and Remark 3.1 given below.

Let e be any edge of an element K. We have that $\boldsymbol{v} \in V_{h,K}^E$ satisfies

$$\int_e \boldsymbol{v}\, d\Gamma = \boldsymbol{0}, \tag{7}$$

and therefore it follows that

$$(\nabla \cdot \boldsymbol{v}, 1)_K = \int_K \nabla \cdot \boldsymbol{v} \, d\Omega = 0 \quad \text{if } \ \boldsymbol{v} \in V^E_{h,K}. \tag{8}$$

The Galerkin formulation of (2) is: Find $(\boldsymbol{u}_h, p_h) \in (V_h, Q_h)$ such that

$$\begin{cases} a_h(\boldsymbol{u}_h, \boldsymbol{v}_h) + b_h(\boldsymbol{v}_h, p_h) & = F(\boldsymbol{v}_h) \qquad \forall\, \boldsymbol{v}_h \in V_h, \\ -b_h(\boldsymbol{u}_h, q_h) & = 0 \qquad\qquad \forall\, q_h \in Q_h, \end{cases} \tag{9}$$

$$a_h(\boldsymbol{u}, \boldsymbol{v}) = 2\mu \sum_{K \in \mathcal{T}_h(\Omega)} (\boldsymbol{\varepsilon}(\boldsymbol{u}), \boldsymbol{\varepsilon}(\boldsymbol{v}))_K \,, \;\; b_h(\boldsymbol{v}, q) = -\sum_{K \in \mathcal{T}_h(\Omega)} (\nabla \cdot \boldsymbol{v}, q)_K \,.$$

We note the formulations (2) and (9) are respectively equivalent to

$$\begin{aligned} a(\boldsymbol{u}, \boldsymbol{v}) &= F(\boldsymbol{v}) \quad \forall\, \boldsymbol{v} \in \mathcal{Z}, \\ a_h(\boldsymbol{u}_h, \boldsymbol{v}_h) &= F(\boldsymbol{v}_h) \quad \forall\, \boldsymbol{v}_h \in \mathcal{Z}_h, \end{aligned}$$

where

$$\begin{aligned} \mathcal{Z} &= \{\boldsymbol{v} \in V \;;\; b(\boldsymbol{v}, q) = 0 \quad \forall\, q \in L^2_0(\Omega)\}, \\ \mathcal{Z}_h &= \{\boldsymbol{v}_h \in V_h \;;\; b_h(\boldsymbol{v}_h, q_h) = 0 \quad \forall\, q_h \in Q_h\}. \end{aligned}$$

Remark 2.1 : The solution $[\boldsymbol{u}, p]$ of (2) is the weak solution associated to (1). If $\boldsymbol{f} \in L^2(\Omega)^2$ and Ω is convex, then there exists a constant $C > 0$ such that $\|\boldsymbol{u}\|_2 + \|p\|_1 \leq C \|\boldsymbol{f}\|$ [15].

Remark 2.2 : Note that (9) is a *non-conforming* method since $V_h \not\subset V$.

3 Inf-sup Condition

The global inf-sup condition is verified with the macroelement technique [20]. A macroelement M_i is a connected region defined as a union of elements K of $\mathcal{T}_h(\Omega)$. In addition it is assumed that the union of all macroelements M_i covers the whole domain Ω. Denote $Q_h(\Sigma)$ and $V^E_{h,\Sigma}$, for $\Sigma = K$ or M, as the spaces given by

$$Q_h(\Sigma) = \{p \in C^0(\Sigma) \;;\; p|_K = \hat{p} \circ F_K^{-1} \;\text{ and }\; \hat{p} \in Q_1(\hat{K}), \forall K \in \Sigma\},$$

and

$$V^E_{h,\Sigma} = \prod_{K \in \Sigma} V^E_{h,K}.$$

Let $|\boldsymbol{v}|_{h,K}^2 = (\boldsymbol{\varepsilon}(\boldsymbol{v}), \boldsymbol{\varepsilon}(\boldsymbol{v}))_K$ and

$$|\boldsymbol{v}|_h^2 = \sum_{K \in \mathcal{T}_h(\Omega)} |\boldsymbol{v}|_{h,K}^2 \, .$$

The macroelement technique [20] allows to verify the following global inf-sup condition,

$$\sup_{\boldsymbol{v}_h \in V_h \setminus \mathbf{0}} \frac{b_h(\boldsymbol{v}_h, q_h)}{|\boldsymbol{v}_h|_h} \geq \beta^* \|q_h\| \quad \forall\, q_h \in Q_h,$$

by fulfilling the following two sufficient conditions:

- If Γ is the common part of the boundaries of two macroelements, then Γ is connected and contains at least two edges of $\mathcal{T}_h(\Omega)$;
- On each macroelement M, the space N_M defined by

$$N_M = \{p \in Q_h(M) \; ; \; (\nabla \cdot \boldsymbol{v}, p)_M = 0 \quad \forall\, \boldsymbol{v} \in V_{h,M}^E\}$$

  is one-dimensional and composed by constant functions.

Meshes topologically equivalent to structured meshes satisfy the second macroelement condition since we can choose families of macroelements formed by 2×2, 3×3, 2×3 and 3×2 elements. This macroelement condition also holds for quadrilateral meshes obtained by connecting triangle barycenters to edge midpoints of a triangular mesh.

We note, by definition, an extension by zero on $\Omega \backslash \Sigma$ of a function in $V_{h,\Sigma}^E$ belongs to V_h^E, and so in V_h. Hence, the spaces $V_{h,K}^E$ and $V_{h,M}^E$ meet the requirements of [20, Lemma 3.2]; that is, $V_{h,K}^E$ and $V_{h,M}^E \subset V_h$.

We prove the following result:

Theorem 3.1 : Let Σ be an element K or a macroelement M. Then the space

$$N_\Sigma = \{p \in Q_h(\Sigma) \; ; \; (\nabla \cdot \boldsymbol{v}, p)_\Sigma = 0 \quad \forall\, \boldsymbol{v} \in V_{h,\Sigma}^E\}$$

is one-dimensional and composed by constant functions.

Proof : We first prove the result for $\Sigma = K$. Let $p = \hat{p} \circ F_K^{-1} \in N_\Sigma$, $\hat{p} = \hat{p}_0 + \hat{p}_1 \hat{x} + \hat{p}_2 \hat{y} + \hat{p}_3 \hat{x}\hat{y}$, and $\boldsymbol{v} = \hat{\boldsymbol{v}} \circ F_K^{-1} = (\hat{v}_1, \hat{v}_2)^t \circ F_K^{-1} \in V_{h,K}^E$. Taking (3) into account, we find

$$\begin{aligned}
(\nabla \cdot \boldsymbol{v}, p)_K \;&=\; \int_{-1}^{1}\int_{-1}^{1} \hat{p} \Big[(c_K^2 + d_K^2 \hat{x}) \frac{\partial \hat{v}_1}{\partial \hat{x}} - (b_K^2 + d_K^2 \hat{y}) \frac{\partial \hat{v}_1}{\partial \hat{y}} \\
&\qquad - (c_K^1 + d_K^1 \hat{x}) \frac{\partial \hat{v}_2}{\partial \hat{x}} + (b_K^1 + d_K^1 \hat{y}) \frac{\partial \hat{v}_2}{\partial \hat{y}} \Big] \, d\hat{x} d\hat{y} \\
&=\; \int_{-1}^{1}\int_{-1}^{1} \hat{p}\, \hat{\nabla} \cdot \Big(J_K B_K^{-1} \hat{\boldsymbol{v}} \Big) \; d\hat{x} d\hat{y} := \hat{b}(\hat{\boldsymbol{v}}, \hat{p}).
\end{aligned}$$

Let us first assume $d_K^1 = d_K^2 = 0$. In this case,

$$\hat{b}(\hat{p}, \hat{\boldsymbol{v}}) = \bar{J}_K \int_{-1}^{1}\int_{-1}^{1} \hat{p}\, \hat{\nabla} \cdot \left((\bar{B}_K)^{-1}\hat{\boldsymbol{v}}\right)\, d\hat{x}d\hat{y}.$$

If $\hat{\boldsymbol{v}} = (\bar{J}_K)^{-1}\bar{B}_K\hat{\boldsymbol{z}}$, then the resulting expression for $\hat{b}(\hat{p}, \hat{\boldsymbol{v}})$ does not depend on F_K:

$$\hat{b}(\hat{p}, \hat{\boldsymbol{v}}) = \int_{-1}^{1}\int_{-1}^{1} \hat{p}\, \hat{\nabla} \cdot \hat{\boldsymbol{z}}\, d\hat{x}d\hat{y}. \tag{10}$$

Defining $\hat{\boldsymbol{z}}_i$ $(i = 1, 2, 3)$ as

$$\hat{\boldsymbol{z}}_1 = \begin{pmatrix} \hat{\phi} \\ 0 \end{pmatrix}, \quad \hat{\boldsymbol{z}}_2 = \begin{pmatrix} 0 \\ \hat{\phi} \end{pmatrix}, \quad \hat{\boldsymbol{z}}_3 = \begin{pmatrix} \hat{y} \\ \hat{x} \end{pmatrix} \hat{\phi},$$

we note from (6) that $\boldsymbol{v} = \hat{\boldsymbol{v}} \circ F_K^{-1} \in V_{h,K}^E$ can be written as

$$\hat{\boldsymbol{v}} = \alpha_K^1 \bar{B}_K \hat{\boldsymbol{z}}_1 + \alpha_K^2 \bar{B}_K \hat{\boldsymbol{z}}_2 + \alpha_K^3 \bar{B}_K \hat{\boldsymbol{z}}_3.$$

Thus, we can choose $\hat{\boldsymbol{v}}_i = (\bar{J}_K)^{-1}\bar{B}_K\hat{\boldsymbol{z}}_i$ $(i = 1, 2, 3)$, which implies $\hat{b}(\hat{p}, \hat{\boldsymbol{v}}_1) = 4p_1/3$, $\hat{b}(\hat{p}, \hat{\boldsymbol{v}}_2) = 4p_2/3$, and $\hat{b}(\hat{p}, \hat{\boldsymbol{v}}_3) = 8p_3/9$. Moreover,

$$\boldsymbol{v} = \frac{3}{4}\left(\hat{p}_1\hat{\boldsymbol{v}}_1 + \hat{p}_2\hat{\boldsymbol{v}}_2 + \frac{3}{2}\hat{p}_3\hat{\boldsymbol{v}}_3\right) \circ F_K^{-1}$$

yields $(\nabla \cdot \boldsymbol{v}, p)_K = \hat{p}_1^2 + \hat{p}_2^2 + \hat{p}_3^2$, which is zero if $\hat{p} = \hat{p}_0$; that is, p is constant.

If $d_K^1 \neq 0$ or $d_K^2 \neq 0$, then $\hat{b}(\hat{p}, \hat{\boldsymbol{v}}_3)$ may depend on $\hat{p}_1$ and $\hat{p}_2$. However, if we choose

$$\hat{\boldsymbol{v}}_4 = \frac{3}{2}\left(\hat{\boldsymbol{v}}_3 - \frac{\hat{b}(\hat{\boldsymbol{v}}_3, \hat{x})}{\hat{b}(\hat{\boldsymbol{v}}_1, \hat{x})}\hat{\boldsymbol{v}}_1 - \frac{\hat{b}(\hat{\boldsymbol{v}}_3, \hat{y})}{\hat{b}(\hat{\boldsymbol{v}}_2, \hat{y})}\hat{\boldsymbol{v}}_2\right) = \frac{3}{2}\hat{\boldsymbol{v}}_3 + \frac{c_K^2 d_K^1 - c_K^1 d_K^2}{10\bar{J}_K}\hat{\boldsymbol{v}}_1 - \frac{b_K^2 d_K^1 - b_K^1 d_K^2}{10\bar{J}_K}\hat{\boldsymbol{v}}_2,$$

then $\hat{b}(\hat{\boldsymbol{v}}_4, \hat{x}) = \hat{b}(\hat{\boldsymbol{v}}_4, \hat{y}) = 0$ and $\hat{b}(\hat{\boldsymbol{v}}_4, \hat{x}\hat{y}) = 4/3$. The choice

$$\boldsymbol{v} = \frac{3}{4}(\hat{p}_1\hat{\boldsymbol{v}}_1 + \hat{p}_2\hat{\boldsymbol{v}}_2 + \hat{p}_3\hat{\boldsymbol{v}}_4) \circ F_K^{-1}$$

yields $(\nabla \cdot \boldsymbol{v}, p)_K = \hat{p}_1^2 + \hat{p}_2^2 + \hat{p}_3^2$, which is zero only if p is constant.

The result for $\Sigma = M$ follows straightforwardly from the case $\Sigma = K$ and the assumption that p is continuous and M is connected. ∎

Remark 3.1 : We find similar analysis and numerical results when we replace $\hat{\boldsymbol{z}}_3 = (\hat{y}\hat{\phi}, \hat{x}\hat{\phi})^t$ to

$$\hat{\boldsymbol{z}}_4 = \begin{pmatrix} \hat{\phi}_1 \\ \hat{\phi}_2 \end{pmatrix}, \quad \hat{\phi}_1(\hat{x},\hat{y}) = \frac{\hat{y}}{8}\left(\frac{\hat{y}^2}{3} - \hat{x}^2\right), \quad \hat{\phi}_2(\hat{x},\hat{y}) = \frac{\hat{x}}{8}\left(\frac{\hat{x}^2}{3} - \hat{y}^2\right),$$

or

$$\hat{\boldsymbol{z}}_5 = \begin{pmatrix} \hat{\phi}_3 \\ \hat{\phi}_4 \end{pmatrix}, \quad \hat{\phi}_3(\hat{x},\hat{y}) = \frac{5\hat{y}^3}{3} + \hat{x}^2\hat{y} - 2\hat{y}, \quad \hat{\phi}_4(\hat{x},\hat{y}) = \frac{5\hat{x}^3}{3} + \hat{y}^2\hat{x} - 2\hat{x}.$$

We note that $\hat{\boldsymbol{z}}_5$ is a linear combination of $\hat{\boldsymbol{z}}_3$ and $\hat{\boldsymbol{z}}_4$. In fact, $y\hat{\phi}$ and $\hat{\phi}_1$ (respectively, $x\hat{\phi}$ and $\hat{\phi}_2$) span all cubic functions with zero average at each side of $\hat{K}$ whose $\hat{x}$-derivative (respectively, $\hat{y}$-derivative) is $C\hat{x}\hat{y}$. Among these functions, $\hat{\psi} = \hat{\phi}_3$ and $\hat{\psi} = \hat{\phi}_4$ are the only ones that satisfy

$$\int_{\hat{e}} \hat{q}\hat{\psi}\, d\Gamma = \mathbf{0}, \quad \forall\, \hat{q} \in P_1(\hat{e}). \tag{11}$$

Property (11) is satisfied by $\hat{\phi}$ as well. If the transformation F_K is linear and $\boldsymbol{v}_i = ((\bar{J}_K)^{-1}\bar{B}_K\hat{\boldsymbol{z}}) \circ F_K^{-1}$ (i=1,2,5), then integrating (10) by parts, follows that

$$(p, \nabla\cdot\boldsymbol{v}_i)_K = -\int_{\hat{K}} \hat{\nabla}\hat{p}\; \hat{\boldsymbol{z}}_i\; d\hat{x}d\hat{y} + \sum_{\hat{e}\in\partial\hat{K}} \int_{\hat{e}} \hat{p}\hat{\boldsymbol{z}}_i \cdot \boldsymbol{n}\, d\Gamma.$$

For $\hat{p} \in Q^1(\hat{K})$, we have that (11) implies

$$\int_{\hat{e}} \hat{p}\hat{\boldsymbol{z}} \cdot \boldsymbol{n}\, d\Gamma = 0. \tag{12}$$

This is one of the conditions required to obtain optimal choices for the P1-P1 non-conforming bubble functions in [19, Eq. (40)]. The second condition, which is

$$\left(q, \nabla\cdot\left(\boldsymbol{a}\hat{\phi}\right)\right)_K = -\boldsymbol{a}\cdot\nabla q \int_K \hat{\phi}\, d\Omega \quad \forall\, q \in Q_1(K), \quad \forall\, \boldsymbol{a} \in I\!R^2,$$

does not hold here, since ∇q may not be constant. When F_K is nonlinear, then (12) does not necessarily hold either.

We finally remark that our theory is based on the property (7). Hence, the theory developed here holds also when we replace $\bar{B}_K$ with B_K in $V_{h,K}^E$; that is,

$$V_{h,K}^E = \left\{\boldsymbol{v}_K \in H^1(K)\; ;\; \boldsymbol{v}_K = B_K\hat{\boldsymbol{z}} \circ F_K^{-1},\; \hat{\boldsymbol{z}} = \begin{pmatrix} \alpha_K^1 \\ \alpha_K^2 \end{pmatrix}\hat{\phi} + \alpha_K^3\boldsymbol{z}_5\right\},$$

since (11) holds and this implies (7). We note that we have tested numerically this later space resulting in similar numerical results as in the case where $V_{h,K}^E$ is given by (6).

Remark 3.2 : Consider the alternative "quadrilateral mini" element of Bai [4, Sec. 4], which employs the enhanced discrete space $V_h^1 \oplus V_h^B$, where

$$V_h^B = \prod_{K \in \mathcal{T}_h(\Omega)} V_{h,K}^B, \qquad V_{h,K}^B = \Big\{ \boldsymbol{v} \in H_0^1(K) \; ; \; \boldsymbol{v}_K = \hat{\boldsymbol{v}} \circ F_K^{-1} \\ \text{and } \; \hat{\boldsymbol{v}} = \begin{pmatrix} \alpha_K^1 + \alpha_K^3(\hat{x}+\hat{y}) \\ \alpha_K^2 + \alpha_K^4(\hat{x}+\hat{y}) \end{pmatrix} \hat{\phi}_b \Big\},$$

where $\hat{\phi}_b(\hat{x},\hat{y}) = (1-\hat{x}^2)(1-\hat{y}^2)$. The argument of Theorem 3.1 can be used to reduce the number of degrees of freedom of each $V_{h,K}^B$ by considering $\tilde{V}_h = V_h^1 \oplus \tilde{V}_h^B$, where

$$\tilde{V}_h^B = \prod_{K \in \mathcal{T}_h(\Omega)} \tilde{V}_{h,K}^B, \qquad \tilde{V}_{h,K}^B = \Big\{ \boldsymbol{v} \in H_0^1(K) \; ; \; \boldsymbol{v}_K = B_K \hat{\boldsymbol{v}} \circ F_K^{-1} \\ \text{and } \; \hat{\boldsymbol{v}} = \begin{pmatrix} \alpha_K^1 \\ \alpha_K^2 \end{pmatrix} \hat{\phi}_b + \alpha_K^3 \begin{pmatrix} \hat{y} \\ \hat{x} \end{pmatrix} \hat{\phi}_b \Big\}, \tag{13}$$

with B_K defined as in (5). On the other hand, if

$$\hat{\boldsymbol{v}} = \begin{pmatrix} \alpha_K^1 \\ \alpha_K^2 \end{pmatrix} \hat{\phi}_b + \alpha_K^3 \nabla \left(\frac{(1-\hat{x})(1-\hat{y})}{4} \right) \hat{\phi}_b,$$

then $\hat{b}(\hat{\boldsymbol{v}}, \hat{x}\hat{y}) = -4\alpha_K^3(b_K^1 + c_K^2)/45$ is zero for instance if $x = \hat{x}$ and $y = -\hat{y}$. This shows that the method proposed in [4, Sec. 3] does not satisfy the macroelement conditions for particular meshes.

4 Error Estimates

The continuous problem (2) satisfies the inf-sup condition, i.e., there exists $\beta > 0$ such that

$$\sup_{\boldsymbol{v} \in V \setminus \boldsymbol{0}} \frac{b_h(\boldsymbol{v}, q)}{|\boldsymbol{v}|_h} \geq \beta \, \|q\| \quad \forall \, q \in Q.$$

In addition, Theorem 3.1 and the macroelement technique [20] lead to a global discrete inf-sup condition; that is, there exists $\beta^* > 0$, that does not depend on h, such that

$$\sup_{\boldsymbol{v}_h \in V_h \setminus \boldsymbol{0}} \frac{b_h(\boldsymbol{v}_h, q_h)}{|\boldsymbol{v}_h|_h} \geq \beta^* \, \|q_h\| \quad \forall \, q_h \in Q_h.$$

We next state some of the well-known results required in the error analysis. The following Poincaré inequalities are valid:

$$\begin{array}{lll} \|\boldsymbol{v}\| & \leq C\,|\boldsymbol{v}|_h & \forall\, \boldsymbol{v} \in V, \\ \|\boldsymbol{v}_K\|_K & \leq Ch\,|\boldsymbol{v}_K|_{h,K} & \forall\, \boldsymbol{v}_K \in V^E_{h,K}, \\ \|\boldsymbol{v}\| & \leq Ch\,|\boldsymbol{v}|_h & \forall\, \boldsymbol{v} \in V^E_h. \end{array}$$

To obtain the first inequality above we have used the fact that functions $\boldsymbol{v} \in V$ vanish on $\partial\Omega$ while the last two inequalities the fact that functions $\boldsymbol{v}_K \in V^E_{h,K}$ or $\boldsymbol{v} \in V^E_h$ have average zero on each edge of $\mathcal{T}_h(\Omega)$. We also have the following stability and approximation results [6, 17]

$$\begin{array}{lll} \|\boldsymbol{v} - \bar{\boldsymbol{v}}\|_{H^{\frac{1}{2}}(e)^2} & \leq C\,|\boldsymbol{v}|_{h,K} & \forall\, \boldsymbol{v} \in V, \\ \inf\limits_{\boldsymbol{c}\in \mathbb{R}^2} \|\boldsymbol{\varepsilon}(\boldsymbol{v})\cdot \boldsymbol{n} - \boldsymbol{c}\|_{H^{-\frac{1}{2}}(e)^2} & \leq Ch\|\boldsymbol{v}\|_{H^2(K)^2} & \forall\, \boldsymbol{v} \in H^2(K)^2, \end{array}$$

where e is any edge of an element K and $\bar{\boldsymbol{v}}$ the edge average of $\boldsymbol{v}$. We remind that $H^{\frac{1}{2}}(e)$ is the half interpolation norm between $H^1(e)$ and $L^2(e)$, and $H^{-\frac{1}{2}}(e)$ the dual norm of $H^{\frac{1}{2}}(e)$ with respect to the $L^2(e)$ norm; see [6, 17].

We next use the following non-conforming FEM theorem [5, page 197]:

$$|\boldsymbol{u} - \boldsymbol{u}_h|_h \leq \inf_{w_h\in \mathcal{Z}_h} |\boldsymbol{u} - \boldsymbol{w}_h|_h + \sup_{w_h\in \mathcal{Z}_h\setminus\{\boldsymbol{0}\}} \frac{a_h(\boldsymbol{u} - \boldsymbol{u}_h, \boldsymbol{w}_h)}{|\boldsymbol{w}_h|_h}. \tag{14}$$

to obtain an optimal approximation on the energy norm for $\boldsymbol{u} - \boldsymbol{u}_h$. The first term on the right-hand-side of (14) is the best approximation error while the second term is the consistency error.

Theorem 4.1 : Assume that $\boldsymbol{u} \in (H^2(\Omega))^2$, $p \in H^1(\Omega) \cap L^2_0(\Omega)$ be the solution of (2). Then the solution $[\boldsymbol{u}_h, p_h]$ of (9) satisfies

$$|\boldsymbol{u} - \boldsymbol{u}_h|_h + \|p - p_h\| \leq Ch(|\boldsymbol{u}|_2 + |p|_1)$$

and if Ω is convex

$$\|\boldsymbol{u} - \boldsymbol{u}_h\| \leq Ch^2(|\boldsymbol{u}|_2 + |p|_1).$$

Proof : We first deal with the consistency error. Let $\boldsymbol{w}_h = \boldsymbol{w}^1_h + \boldsymbol{w}^E_h \in \mathcal{Z}_h$, where $\boldsymbol{w}^1_h \in V^1_h$ and $\boldsymbol{w}^E_h \in V^E_h$. Then

$$\begin{array}{rcl} a_h(\boldsymbol{u} - \boldsymbol{u}_h, \boldsymbol{w}_h) & = & a_h(\boldsymbol{u}, \boldsymbol{w}_h) - a_h(\boldsymbol{u}_h, \boldsymbol{w}_h) \\ & = & a_h(\boldsymbol{u}, \boldsymbol{w}_h) - F(\boldsymbol{w}_h) \\ & = & b_h(\boldsymbol{w}_h, \Pi p - p) + b_h(\boldsymbol{w}_h, p) + a_h(\boldsymbol{u}, \boldsymbol{w}_h) - F(\boldsymbol{w}_h), \end{array}$$

where Πp is the L_2 projection of p on Q_h. Hence,

$$
\begin{aligned}
|a_h(\boldsymbol{u}-\boldsymbol{u}_h,\boldsymbol{w}_h)| &\leq |b_h(\boldsymbol{w}_h, p-\Pi p)| + |a_h(\boldsymbol{u},\boldsymbol{w}_h) - F(\boldsymbol{w}_h) + b_h(\boldsymbol{w}_h, p)| \\
&\leq \sqrt{2}\,\|p-\Pi p\|\,|\boldsymbol{w}_h|_h + \Bigg| \sum_{K\in\mathcal{T}_h(\Omega)} 2\mu \int_K \boldsymbol{\varepsilon}(\boldsymbol{u}) : \boldsymbol{\varepsilon}(\boldsymbol{w}_h)\, d\Omega - \int_K \boldsymbol{f}\cdot\boldsymbol{w}_h\, d\Omega \\
&\quad - \int_K p\nabla\cdot\boldsymbol{w}_h\, d\Omega \Bigg| \\
&\leq Ch\,|p|_1\,|\boldsymbol{w}_h|_h + \Bigg| \sum_{K\in\mathcal{T}_h(\Omega)} \int_K (-2\mu\nabla\cdot\boldsymbol{\varepsilon}(\boldsymbol{u}) + \nabla p - \boldsymbol{f})\cdot\boldsymbol{w}_h\, d\Omega \\
&\quad + \sum_{K\in\mathcal{T}_h(\Omega)} 2\mu \int_{\partial K} \boldsymbol{w}_h\cdot(\boldsymbol{\varepsilon}(\boldsymbol{u})\cdot\boldsymbol{n})\, d\Gamma - \int_{\partial K} p\boldsymbol{w}_h\cdot\boldsymbol{n}\, d\Gamma \Bigg|.
\end{aligned}
$$

Note that the second term of the right-hand side vanishes because $[\boldsymbol{u}, p]$ satisfies (1). Moreover, we have

$$
\begin{aligned}
&\Bigg| \sum_{K\in\mathcal{T}_h(\Omega)} 2\mu \int_{\partial K} \boldsymbol{w}_h\cdot(\boldsymbol{\varepsilon}(\boldsymbol{u})\cdot\boldsymbol{n})\, d\Gamma - \int_{\partial K} p\boldsymbol{w}_h\cdot\boldsymbol{n}\, d\Gamma \Bigg| \\
&= \Bigg| \sum_{e\in\mathcal{T}_h(\Omega)} 2\mu \int_e [\boldsymbol{w}_h]\cdot(\boldsymbol{\varepsilon}(\boldsymbol{u})\cdot\boldsymbol{n})\, d\Gamma - \int_e p[\boldsymbol{w}_h]\cdot\boldsymbol{n}\, d\Gamma \Bigg|,
\end{aligned}
$$

where $[\boldsymbol{w}_h]$ is the jump of $\boldsymbol{w}_h$ across an interior edge e of $\mathcal{T}_h(\Omega)$ or $[\boldsymbol{w}_h] = \boldsymbol{w}_h$ on a boundary edge e of $\mathcal{T}_h(\partial\Omega)$. In both cases $[\boldsymbol{w}_h]$ have zero average on e. For the case where the edge e is an interior edge and K_e^r and K_e^l are the two elements sharing this edge, we obtain

$$
\begin{aligned}
\left| \int_e [\boldsymbol{w}_h]\cdot(\boldsymbol{\varepsilon}(\boldsymbol{u})\cdot\boldsymbol{n})\, d\Gamma \right| &= \inf_{\boldsymbol{c}\in I\!R^2} \left| \int_e [\boldsymbol{w}_h]\cdot(\boldsymbol{\varepsilon}(\boldsymbol{u})\cdot\boldsymbol{n} - \boldsymbol{c})\, d\Gamma \right| \\
&\leq \inf_{\boldsymbol{c}\in I\!R^2} \|\boldsymbol{\varepsilon}(\boldsymbol{u})\cdot\boldsymbol{n} - \boldsymbol{c}\|_{-1/2,e}\, \|[\boldsymbol{w}_h]\|_{1/2,e} \\
&\leq Ch\,\|\boldsymbol{u}\|_{2,K_e^l}\,\|[\boldsymbol{w}_h]\|_{1/2,e} \\
&\leq Ch\,\|\boldsymbol{u}\|_{2,K_e^l}\,(\|\boldsymbol{w}_h - \bar{\boldsymbol{w}}_h^e\|_{h,K_e^l} + \|\boldsymbol{w}_h - \bar{\boldsymbol{w}}_h^e\|_{h,K_e^r}) \\
&\leq Ch\,\|\boldsymbol{u}\|_{2,K_e^l}\,|\boldsymbol{w}_h|_{h,K_e^l\cup K_e^r}\,.
\end{aligned}
$$

On the the first inequality above we have used standard $H^{-1/2}$ approximation results on a element level. On the last inequality we have used a Poincaré inequality on the two elements K_e^l and K_e^r sharing the edge e, where $\bar{\boldsymbol{w}}_h^e$ is the average of $\boldsymbol{w}_h$ on e. Using similar arguments we also obtain

$$\left| \int_e p[\boldsymbol{w}_h] \cdot \boldsymbol{n} \, d\Gamma \right| \quad \leq \quad Ch \, |p|_{1,K_e^l} \, |\boldsymbol{w}_h|_{h,K_e^l \cup K_e^r} \, .$$

Similar bounds hold for $e \in \partial\Omega$ since $\boldsymbol{w}_h$ has average zero ($\boldsymbol{w}_h^1$ vanishes on $\partial\Omega$). Adding all the contributions and using that u vanishes on $\partial\Omega$, we obtain

$$\sup_{\boldsymbol{w}_h \in \mathcal{Z}_h \setminus \boldsymbol{0}} \frac{|a_h(\boldsymbol{u} - \boldsymbol{u}_h, \boldsymbol{w}_h)|}{|\boldsymbol{w}_h|_h} \leq Ch(|\boldsymbol{u}|_2 + |p|_1).$$

The best approximation error of the velocity is obtained as follows. Let Π_1 be the L^2 projector on V_h^1. Using Theorem 1.1 ([15], page 114) and standard L_2 projection approximation, we obtain

$$\begin{aligned} \inf_{\boldsymbol{w}_h \in \mathcal{Z}_h} |\boldsymbol{u} - \boldsymbol{w}_h|_h \quad &\leq \quad (1 + \frac{\|b\|}{\beta^*}) \inf_{\boldsymbol{v}_h \in V_h} |\boldsymbol{u} - \boldsymbol{v}_h|_h \\ &\leq \quad C \, |\boldsymbol{u} - \Pi_1 \boldsymbol{u}|_h \leq Ch \, |\boldsymbol{u}|_2 \, . \end{aligned}$$

We next show that

$$\|p - p_h\| \leq Ch(|\boldsymbol{u}|_2 + |p|_1).$$

Indeed, for all $q_h \in Q_h$ and $\boldsymbol{v}_h \in V_h$, we have

$$\begin{aligned} b_h(\boldsymbol{v}_h, p_h - q_h) \quad = \quad & a_h(\boldsymbol{u} - \boldsymbol{u}_h, \boldsymbol{v}_h) + b_h(\boldsymbol{v}_h, p - q_h) - \\ & \sum_{K \in \mathcal{T}_h(\Omega)} \sum_{e \in \partial K} \left(\int_e 2\mu \boldsymbol{v}_h \cdot (\boldsymbol{\varepsilon}(\boldsymbol{u}) \cdot \boldsymbol{n}) \, d\Gamma - \int_e p \boldsymbol{v}_h^E \cdot \boldsymbol{n} \, d\Gamma \right) . \end{aligned}$$

And using the inf-sup condition for the discrete formulation and similar error analysis used above we obtain:

$$\begin{aligned} \|p_h - q_h\| \quad &\leq \quad \frac{1}{\beta^*} \max_{\boldsymbol{v}_h \in V_h} \frac{|b_h(\boldsymbol{v}_h, p_h - q_h)|}{|\boldsymbol{v}_h|_h} \\ &\leq \quad \frac{1}{\beta^*} \left[|\boldsymbol{u} - \boldsymbol{u}_h|_h + C \left(\|p - q_h\| + h \, |\boldsymbol{u}|_2 + h \, |p|_1 \right) \right] . \end{aligned}$$

Finally, choosing $q_h = \Pi p$ and using the triangular inequality, we obtain:

$$\|p - p_h\| \leq \|p - q_h\| + \|q_h - p_h\| \leq \frac{1}{\beta^*} Ch(|\boldsymbol{u}|_2 + |p|_1).$$

The L^2-error estimate for $\boldsymbol{u} - \boldsymbol{u}_h$ follows straightforwardly from the Aubin-Nitsche trick. ∎

We next show that we can remove the component $\boldsymbol{u}_h^E$ from the solution $\boldsymbol{u}_h$ and still obtain optimal error estimates. Hence, the proposed enriched finite element discretization can be considered as a stabilized finite element method since the enriched basis functions can be statically condensed at the element level.

Theorem 4.2 : Assume that $\boldsymbol{u} \in (H^2(\Omega))^2$, $p \in H^1(\Omega) \cap L_0^2(\Omega)$ be the solution of (2) and $[\boldsymbol{u}_h, p_h]$ solution of (9) with $\boldsymbol{u}_h = \boldsymbol{u}_h^1 + \boldsymbol{u}_h^E$, $\boldsymbol{u}_h^1 \in V_h^1$ and $\boldsymbol{u}_h^E \in V_h^E$. Then,

$$\left|\boldsymbol{u} - \boldsymbol{u}_h^1\right|_h \leq Ch(|\boldsymbol{u}|_2 + |p|_1)$$

and if Ω is convex

$$\left\|\boldsymbol{u} - \boldsymbol{u}_h^1\right\| \leq Ch^2(|\boldsymbol{u}|_2 + |p|_1).$$

Proof : Using the linear independence between the spaces $V_h^1(K)$ and $V_{h,k}^E$ and quasi-uniformity and regularity assumptions of $\mathcal{T}_h(\Omega)$, it is not hard to see that there exists $\alpha < 1$ such that

$$\left(\boldsymbol{\varepsilon}(\boldsymbol{u}_h^1), \boldsymbol{\varepsilon}(\boldsymbol{u}_h^E)\right)_K \leq \alpha \left|\boldsymbol{u}_h^1\right|_{h,K} \left|\boldsymbol{u}_h^E\right|_{h,K}$$

for any element $K \in \mathcal{T}_h$. It follows that

$$\left(\boldsymbol{\varepsilon}(\boldsymbol{u}_h^1), \boldsymbol{\varepsilon}(\boldsymbol{u}_h^E)\right) \leq \alpha \left|\boldsymbol{u}_h^1\right|_h \left|\boldsymbol{u}_h^E\right|_h$$

and

$$\left|\boldsymbol{u}_h^E\right|_h^2 + \left|\boldsymbol{u}_h^1\right|_h^2 \leq \frac{1}{1-\alpha} \left|\boldsymbol{u}_h^E + \boldsymbol{u}_h^1\right|_h^2. \tag{15}$$

Let $\boldsymbol{u}^I$ be the bilinear interpolant of $\boldsymbol{u}$. We have from (15) that

$$\begin{aligned}
\left|\boldsymbol{u}_h^E\right|_h^2 + \left|\boldsymbol{u}_h^1 - \boldsymbol{u}^I\right|_h^2 &\leq \frac{1}{1-\alpha} \left|\boldsymbol{u}_h - \boldsymbol{u}_h^I\right|_h^2 \\
&\leq \frac{2}{1-\alpha} \left(|\boldsymbol{u}_h - \boldsymbol{u}|_h^2 + \left|\boldsymbol{u} - \boldsymbol{u}_h^I\right|_h^2\right) \\
&\leq Ch^2(|\boldsymbol{u}|_2^2 + |p|_1^2) + Ch^2 \, |\boldsymbol{u}|_2^2 .
\end{aligned}$$

The energy estimate follows from the triangular inequality

$$\left|\boldsymbol{u} - \boldsymbol{u}_h^1\right|_h \leq |\boldsymbol{u} - \boldsymbol{u}_h|_h + \left|\boldsymbol{u}_h^E\right|_h^2 .$$

The L_2 error estimate can be obtained using similar arguments. ∎

5 Numerical Experiments

Consider two test problems with $\mu = 1$ on meshes of n^2 elements, $n = 20, 40, 80$ (Fig. 1). The first mesh (M1) is asymptotically affine [1] and the second mesh (M2) is non-affine. Mesh M1 allows us to assess the methods on non-rectangular meshes which are nearly affine-equivalent [9, Sec. 2.4]. Mesh M2 is generated from a square mesh by translating the center of each 2×2 macroelement $h/2$ to the right and $h/4$ to the top.

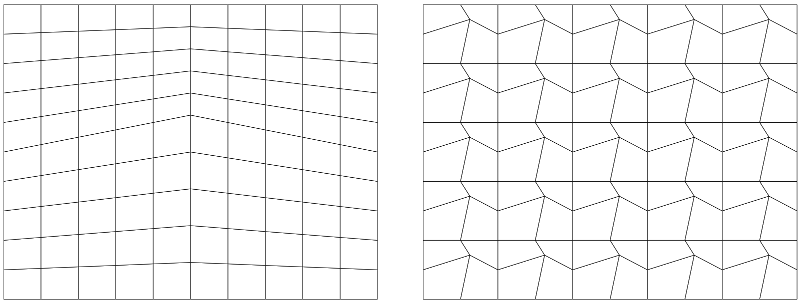

Figure 1: Meshes M1 (left) and M2 (right) for $\Omega = (-1, 1)^2$

The values of $\|p - p_h\|$, $\|\boldsymbol{u} - \boldsymbol{u}_h\|$, $|\boldsymbol{u} - \boldsymbol{u}_h|_h$, and $\|\nabla \cdot \boldsymbol{u}_h\|$ of the proposed method are computed and compared with the errors of the Galerkin Least-Squares method [11]:

$$\left\{ \begin{array}{llll} a(\boldsymbol{u}_h, \boldsymbol{v}_h) + b(\boldsymbol{v}_h, p_h) & - (\mathcal{L}[\boldsymbol{u}_h, p_h] - \boldsymbol{f}, \tau_1 \mathcal{L}[\boldsymbol{v}_h, q_h])_{\tilde{\Omega}} & = F(\boldsymbol{v}_h) & \forall\, \boldsymbol{v}_h \in V_h^1, \\ -b(\boldsymbol{u}_h, q_h) & - (\nabla \cdot \boldsymbol{u}_h, \tau_2 \nabla \cdot \boldsymbol{v}_h)_{\tilde{\Omega}} & = 0 & \forall\, q_h \in Q_h, \end{array} \right. \tag{16}$$

where $\mathcal{L}[\boldsymbol{u}_h, p_h] = -2\mu \nabla \cdot \boldsymbol{\varepsilon}(\boldsymbol{u}) + \nabla p$ and the stabilization parameters $\tau_{1,2}$ as in [10, 12]:

$$\tau_1 = \frac{(h^e)^2}{24\mu} \qquad \tau_2 = 12\mu.$$

We also present the error curves for the enriched method when the component $\boldsymbol{u}_h^E$ is removed from the solution $\boldsymbol{u}_h$. We identify each method in the figures below as follows:

GLS: Galerkin Least-Squares method (16);
E_NC: Method (9) enhanced by the non-conforming field (6);
E_NC1: Component $\boldsymbol{u}_h^1$ of the approximate solution by the method "E_NC".

The order of convergence of each method is estimated by linear regression of the logarithm of the computed errors and is shown in the figure captions.

5.1 Smooth Velocity-pressure Field

We first consider the problem employed in [9]: let $\Omega = (-1,1)^2$ and select the right-hand side such that the exact solution is

$$\begin{aligned} u_1(x,y) &= -e^x(y\cos y + \sin y), \\ u_2(x,y) &= e^x y \sin y, \\ p(x,y) &= 2e^x \sin y. \end{aligned}$$

The errors shown in Figs. 2-5 meet the theoretical predictions. The method "E_NC1" has slightly better results than the Galerkin least-squares method; an additional improvement is noticed when the enrichment field is taken into account ("E_NC"). "E_NC" has shown to be more conservative, i.e., it has the lowest divergence error. The pressure error of "E_NC" in the L^2 norm has also been lower than in GLS.

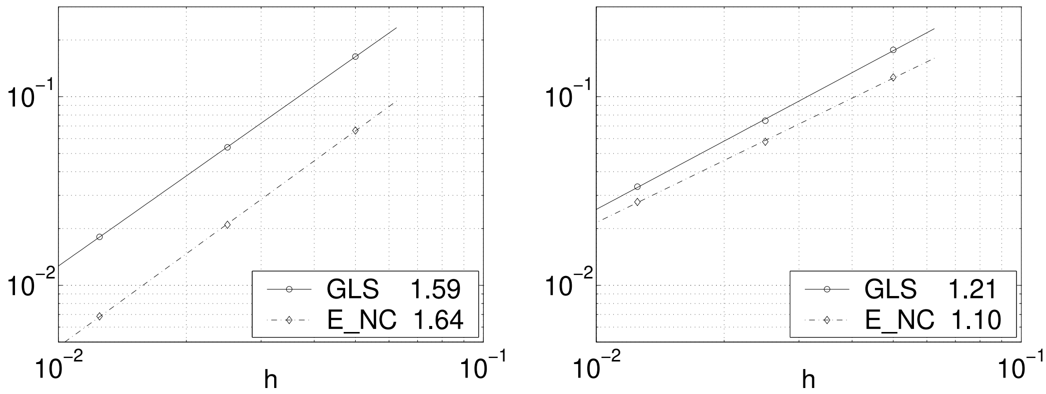

Figure 2: Graphs of $\|p - p_h\|$ for Prob. 5.1, mesh M1 (left) and mesh M2 (right)

Remark 5.1 : The performance of "E_NC" is similar to the performance of the methods proposed in [4], as well as the improved "quadrilateral mini" element proposed on Remark 3.2, except that "E_NC" had a more accurate approximation of the pressure and the divergence of the velocity, as shown in Fig. 6. In this figure,

E_C: Method (9) enhanced by the conforming field (13);
E_C1: Component $\boldsymbol{u}_h^1$ of the approximate solution by the method "E_C".

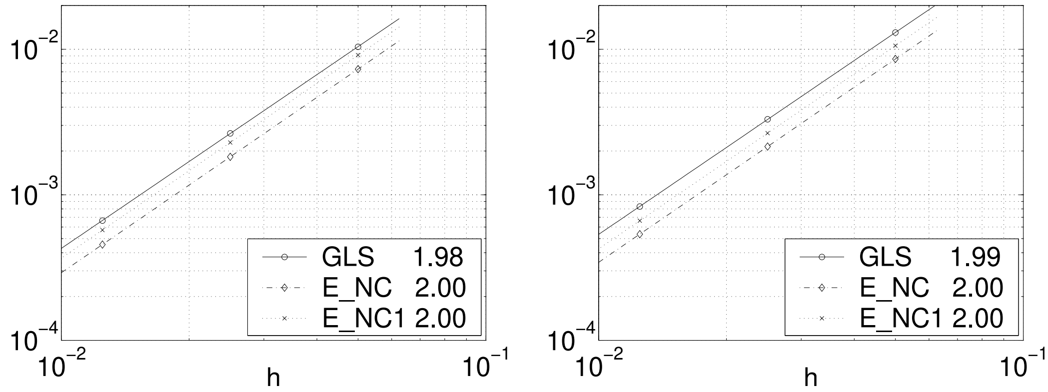

Figure 3: Graphs of $\|\boldsymbol{u} - \boldsymbol{u}_h\|$ for Prob. 5.1, mesh M1 (left) and mesh M2 (right)

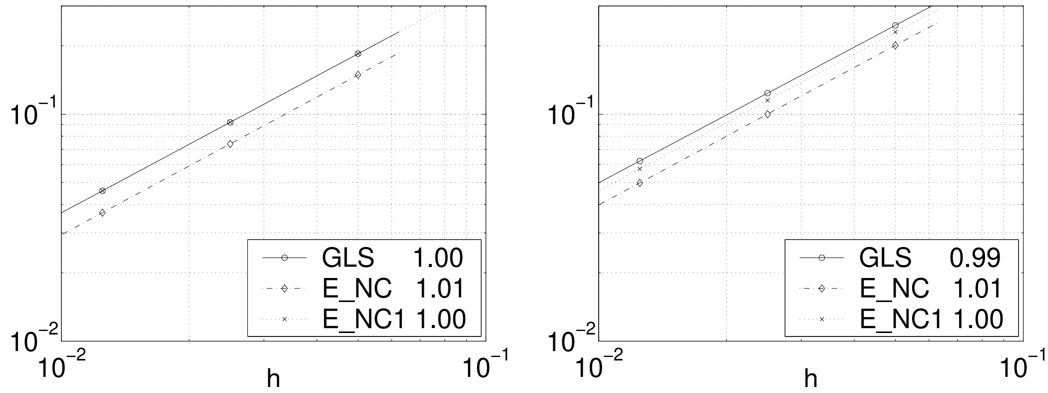

Figure 4: Graphs of $|\boldsymbol{u} - \boldsymbol{u}_h|_h$ for Prob. 5.1, mesh M1 (left) and mesh M2 (right)

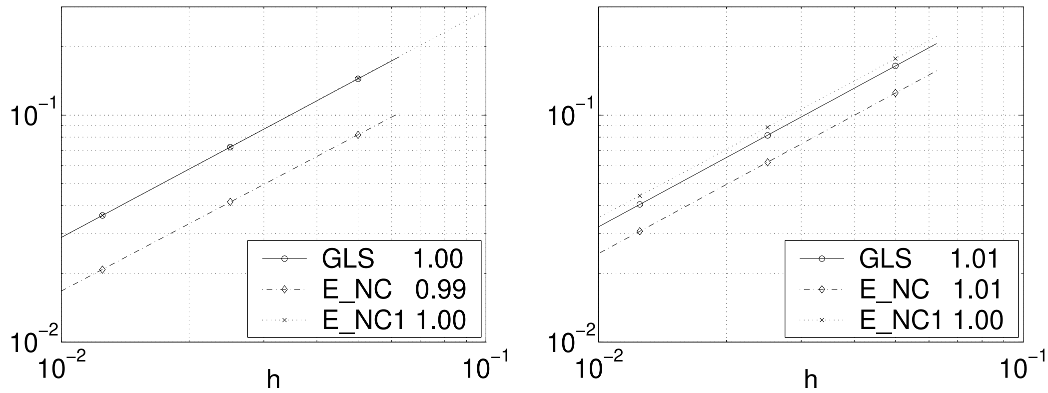

Figure 5: Graphs of $\|\nabla \cdot \boldsymbol{u}_h\|$ for Prob. 5.1, mesh M1 (left) and mesh M2 (right)

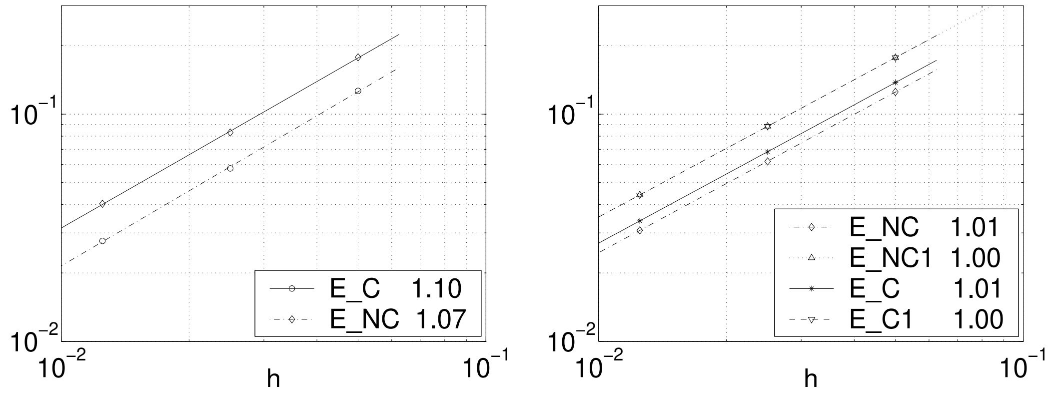

Figure 6: Graphs of $\|p - p_h\|$ (left) and $\|\nabla \cdot \boldsymbol{u}_h\|$ (right) for Prob. 5.1, mesh M2.

5.2 Driven Cavity Flow

We consider the driven cavity problem in $\Omega = (0,1)^2$ with a "leaky lid" boundary condition [16] of the same length as the element of the coarser uniform mesh (Fig. 7). This benchmark problem models the laminar incompressible flow in a square cavity whose top wall moves with a uniform velocity [14].

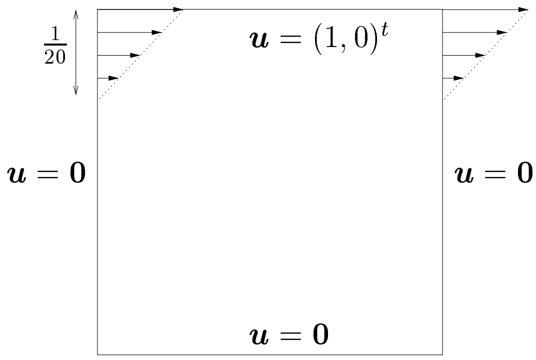

Figure 7: Statement of Prob. 5.2

Figs. 8-11 present the errors with respect to the solution by the "E_NC" method in a mesh of 200x200 squares. We note that "E_NC" provided the best pressure approximation also in this problem.

Remark 5.2 :
According to Remark 3.2, the method proposed in [4, Sec. 3] may experience difficulties for certain meshes. This is confirmed by Fig. 12, which compares the pressure

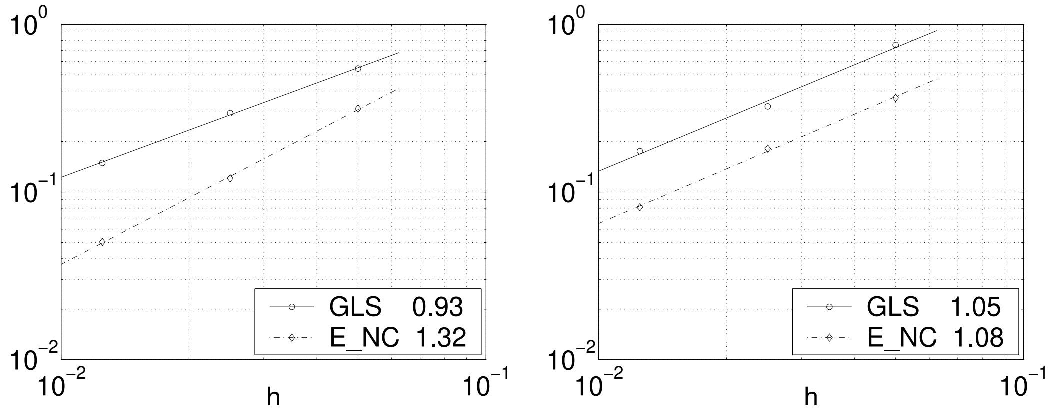

Figure 8: Graphs of $\|p - p_h\|$ for Prob. 5.2, mesh M1 (left) and mesh M2 (right)

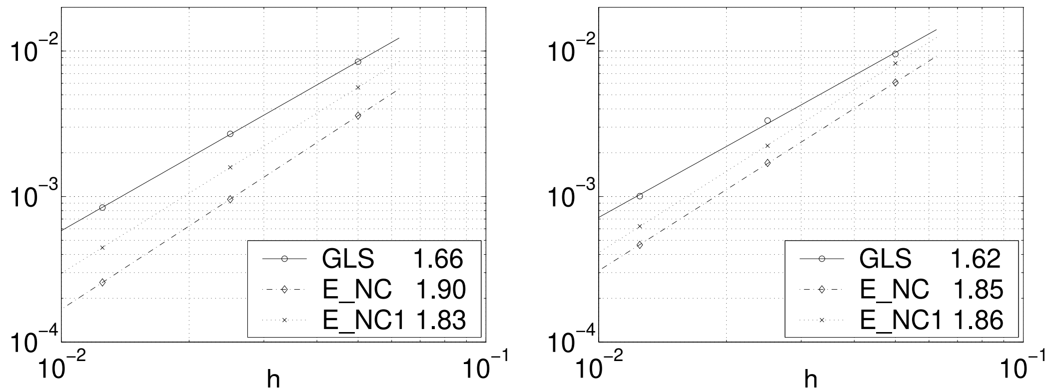

Figure 9: Graphs of $\|\boldsymbol{u} - \boldsymbol{u}_h\|$ for Prob. 5.2, mesh M1 (left) and mesh M2 (right)

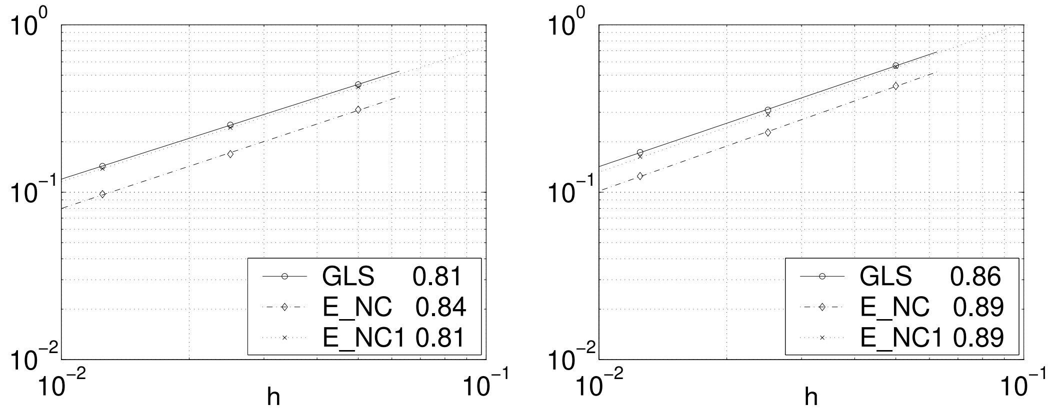

Figure 10: Graphs of $|\boldsymbol{u} - \boldsymbol{u}_h|_h$ for Prob. 5.2, mesh M1 (left) and mesh M2 (right)

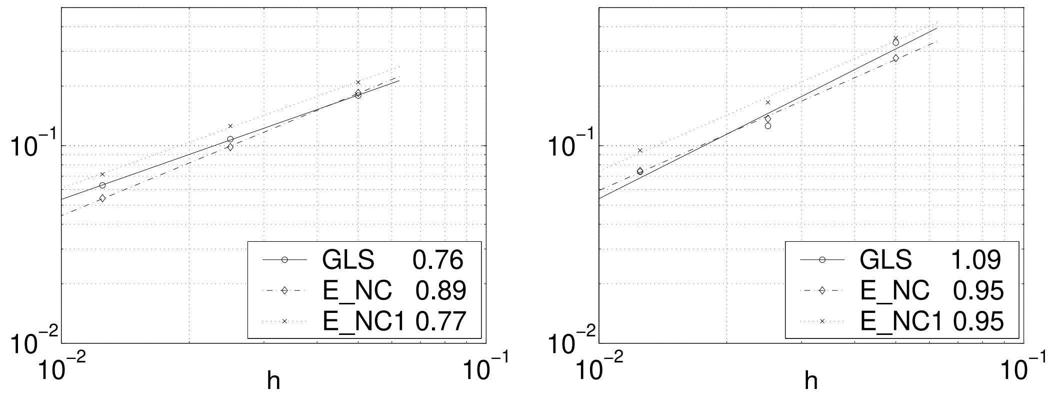

Figure 11: Graphs of $\|\nabla \cdot \boldsymbol{u}_h\|$ for Prob. 5.2, mesh M1 (left) and mesh M2 (right)

field of this method and the improved "quadrilateral mini" element for a mesh of 20×20 square elements numbered from the upper left corner to the lower right corner (see also [18, Fig. 5]).

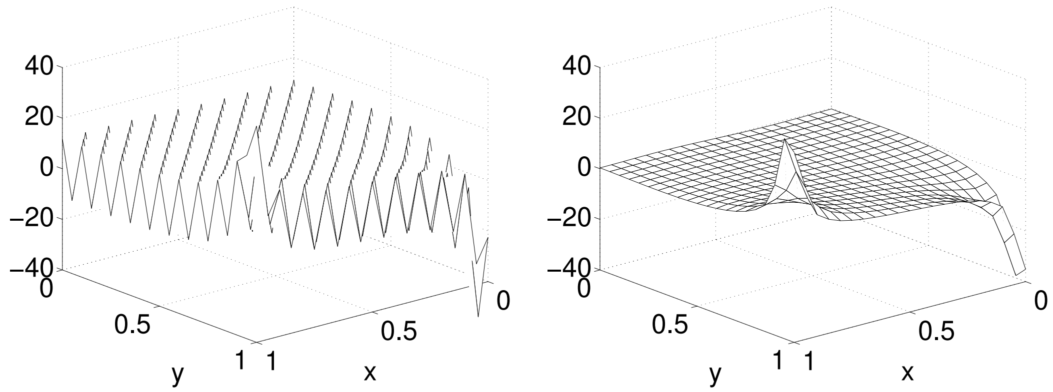

Figure 12: Pressure elevation plots of p_h for the method proposed in [4, Sec. 3] (left) and the method "E_C" (right).

6 Conclusions

We propose a stabilization of the Q1-Q1 element with the aid of polynomial, non-conforming bubble functions which extends the work presented in [4]. The proof of the inf-sup condition serves as a framework for validating other enriched finite-element pairs. Numerical experiments confirm the error estimates and also verifies that the proposed method is highly conservative and provides an accurate approximation of the pressure field.

References

[1] D. N. Arnold, D. Boffi, and R. S. Falk. Approximation by quadrilateral finite elements. *Mathematics of Computation*, 71(239):909–922, 2002.

[2] D. N. Arnold, F. Brezzi, and M. Fortin. A stable finite element for the Stokes equations. *Calcolo*, 21(4):337–344, 1984.

[3] I. Babuška. The finite element method with Lagrangian multipliers. *Numerische Mathematik*, 20:179–192, 1973.

[4] W. Bai. The quadrilateral "Mini" finite element for the Stokes problem. *Computer Methods in Applied Mechanics and Engineering*, 143(1-2):41–47, 1997.

[5] S. C. Brenner and L. R. Scott. *The mathematical theory of finite element methods*. Springer-Verlag, New York, 1994.

[6] F. Brezzi. On the existence, uniqueness and approximation of saddle-point problems arising from Lagrangian multipliers. *Revue Française d'Automatique Informatique et Recherche Opérationnelle, Série Rouge*, 8(R-2):129–151, 1974.

[7] F. Brezzi and M. Fortin. *Mixed and hybrid finite element methods*. Springer-Verlag, New York, 1991.

[8] F. Brezzi and J. Pitkäranta. On the stabilization of finite element approximations of the Stokes equations. In *Efficient Solutions of Elliptic Systems (Kiel, 1984)*, pages 11–19. Vieweg, Braunschweig, 1984.

[9] B. Cockburn, G. Kanschat, D. Schötzau, and C. Schwab. Local discontinuous Galerkin methods for the Stokes problem. *SIAM Journal of Numerical Analysis*, 40(1):319–343, 2002.

[10] L. Franca and S. Frey. Stabilized finite element methods: II. the incompressible Navier-Stokes equations. *Computer Methods in Applied Mechanics and Engineering*, 99(2–3):209–233, 1992.

[11] L. P. Franca and T. J. R. Hughes. Two classes of mixed finite element methods. *Computer Methods in Applied Mechanics and Engineering*, 69(1):89–129, 1988.

[12] L. P. Franca and T. J. R. Hughes. Convergence analyses of Galerkin least-squares methods for symmetric advective-diffusive form of the Stokes and incompressible

Navier-Stokes equations. *Computer Methods in Applied Mechanics and Engineering*, 105(2):285–298, 1993.

[13] L. P. Franca, T. J. R. Hughes, and R. Stenberg. Stabilized finite element methods for the Stokes problem. In M. Gunzburger and R. Nicolaides, editors, *Incompressible Computational Fluid Dynamics - Trends and Advances*, chapter 4. Cambridge University Press, Cambridge, UK, 1993.

[14] U. Ghia, K. N. Ghia, and C. T. Shin. High-Re solutions for incompressible flow using the the Navier-Stokes equations and a multigrid method. *Journal of Computational Physics*, 48:387–411, 1982.

[15] V. Girault and P.-A. Raviart. *Finite element methods for Navier-Stokes equations - theory and algorithms.* Springer–Verlag, Berlim, 1986.

[16] T. J. R. Hughes, L. P. Franca, and M. Balestra. A new finite element formulation for computational fluid dynamics. V. Circumventing the Babuška-Brezzi condition: a stable Petrov-Galerkin formulation of the Stokes problem accommodating equal-order interpolations. *Computer Methods in Applied Mechanics and Engineering*, 59(1):85–99, 1986.

[17] B. Khoromskij and G. Wittum. *Numerical solution of elliptic differential equations by reduction to the interface*, volume 36. Springer-Verlag, 2004.

[18] P. Mons and G. Rogé. L'élément Q_1-bulle/Q_1. *M2AN. Mathematical Modelling and Numerical Analysis*, 26(4):507–521, 1992.

[19] R. Pierre. Optimal selection of the bubble function in the stabilization of the P1-P1 element for the Stokes problem. *SIAM Journal on Numerical Analysis*, 32(4):1210–1224, 1995.

[20] R. Stenberg. Analysis of mixed finite elements methods for the Stokes problem: a unified approach. *Mathematics of Computation*, 42(165):9–23, 1984.